Theoretical investigation on the electronic structures and phosphorescent properties of a series of cyclometalated platinum(II) complexes with different substituted N-heterocyclic carbene ligands

Deming Han, Xiuxia He, Lihui Zhao, Chunying Pang, Yuanhua Yu & Gang Zhang

Published online: 19 Feb 2016.

Submit your article to this journal

Article views: 85

View related articles

View Crossmark data

Taylor & Francis
Taylor & Francis Group

Theoretical investigation on the electronic structures and phosphorescent properties of a series of cyclometalated platinum(II) complexes with different substituted N-heterocyclic carbene ligands

Deming Han[a], Xiuxia He[a], Lihui Zhao[a], Chunying Pang[a], Yuanhua Yu[a], and Gang Zhang[b]

[a]School of Life Science and Technology, Changchun University of Science and Technology, Changchun, Jilin, P. R. China; [b]State Key Laboratory of Theoretical and Computational Chemistry, Institute of Theoretical Chemistry, Jilin University, Changchun, Jilin, P. R. China

ABSTRACT

A series of substituted platinum(II) complexes with a chelating N-heterocyclic carbene (NHC) ligand and a bidentate monoanionic auxiliary ligand (acetylacetone) have been investigated by using the density functional theory (DFT) and time-dependent density functional theory (TDDFT) methods, to explore their electronic structures, absorption and emission properties, and phosphorescence quantum efficiency. The influence of different substituted groups on photophysical properties of complexes studied has been detailedly analyzed. The lowest energy absorption and emission wavelengths calculated are comparable to the available experimental values. In addition, ionization potential (IP), electron affinities (EA), and reorganization energy (λ) were obtained to evaluate the charge transfer and balance properties between hole and electron. The calculated results also show that, due to a lower $\Delta E_{S_1-T_1}$, larger ^{3}MLCT contribution, and higher μ_{S_1} value, the complex **5** owns possibly the largest k_r value among these complexes. The theoretical studies could provide useful information for the candidated phosphorescent platinum(II) material for use in the organic light-emitting diodes.

1. Introduction

In the past two decades, phosphorescent dopants with d^6 and d^8 transition metal as core atom have been extensively investigated for the design and synthesis of good materials in organic light-emitting diodes (OLEDs) [1–6]. Theoretically, the internal quantum yield of phosphorescent complexes could reach 75% statistically and even to 100% on the basis of a fast intersystem crossing (ISC) from singlets to triplets or by harvesting both fluorescent and phosphorescent emissions. In recent years, many Pt(II) complexes with bidentate cyclometalated or tridentate ligands have been synthesized and investigated for the potential applications as OLEDs materials [7–15]. For example, Mark E. Thompson et al. have investigated the photophysical properties of a series of square planar Pt(II) complexes with the general structure,

(C^N)Pt(O^O), where O^O is a β-diketonate ligand, i.e., acetyl acetonate (acac) or dipivolyl-methane (dpm) [16]. Swager and co-workers have reported their study on a series of Pt(II) complexes containing bidentate ligands as potential phosphorescent reporters of cyanogen halides via an oxidative addition reaction [17]. It is well-known that Pt(II) complexes with a d^8 electronic configuration are typical phosphorescent material due to the square-planar structure, which facilitates the electron–hole creation and separation. Besides, Pt(II) complexes containing aromatic N-donor and/or cyclometalated ligands have various emissive excited states nature, including metal to ligand charge transfer (MLCT), ligand to ligand charge transfer (LLCT), intraligand charge transfer (ILCT) and so on.

Recently, the C^C cyclometalated Pt(II) complexes with N-heterocyclic carbene (NHC) ligands have been studied as potential emitter materials in OLEDs, which possess good quantum yields, colour and stability [18, 19] In this paper, five C^C cyclometalated Pt(II) complexes with NHC ligands and substituted phenyl ring have been investigated by using the density functional theory (DFT) and time-dependent density functional theory (TDDFT). The electronic structures, charge injection, and transport, and spectral properties of these complexes have been investigated. It is anticipated that the study can provide a good guidance for the synthesis of new platinum complexes suited to phosphorescence emitter in electroluminescent layered structure.

2. Computational details

The ground state geometry for each molecule was optimized by the DFT method with Becke's three parameter hybrid method combined with the Lee–Yang–Parr correlation functional (denoted as B3LYP) [20–22]. The geometry optimizations of the lowest triplet states (T_1) were performed by unrestricted B3LYP approach. On the basis of the ground- and excited-state equilibrium geometries, the time-dependent DFT (TDDFT) approach associated with the SCRF (self-consistent reaction field) theory using the integral equation formalism polarized continuum model (IEFPCM) [23,24] in dichloromethane (CH_2Cl_2) medium was applied to investigate the absorption and emission spectral properties. The equilibrium solvation regime is employed for the geometry optimization of the solute molecule in the ground and excited states, while the nonequilibrium solvation regime is employed for vertical transitions. The "double-ξ" quality basis set LANL2DZ associated with the pseudopotential was employed on atom Pt [25,26]. The 6−31+G(d) basis set was used for nonmetal atoms in the gradient optimizations. Furthermore, the stable configurations of these complexes can be confirmed by frequency analysis, in which no imaginary frequency was found for all configurations at the energy minima. In addition, the positive and negative ions with regard to the "electron-hole" creation are relevant to their use as OLEDs materials. Thus, ionization potentials (IP), electron affinities (EA), and reorganization energy (λ) were obtained by comparing the energy levels of neutral molecule with positive ions and negative ions, respectively. The calculated electronic density plots for frontier molecular orbitals were prepared by using the GaussView 5.0.8 software. The absorption spectra were simulated by using the GaussSum 2.5 software [27] with the full width at half maximum (FWHM) of 3000 cm^{-1} based on the present TDDFT computational results. All calculations were performed with the Gaussian 09 software package [28].

3. Results and discussion

3.1. Geometries in the ground state S_0 and triplet excited state T_1

The sketch map of the five complexes **1**, **2**, **3**, **4**, and **5** (**1**−**5** denotes these studied complexes from **1** to **5**, the same hereafter) are presented in Fig. 1a, and the optimized ground state

a

1 : R1 = H   R2 = CN
2 : R1 = CN   R2 = CN
3 : R1 = CF$_3$ R2 = CF$_3$
4 : R1 = CH$_3$ R2 = CH$_3$
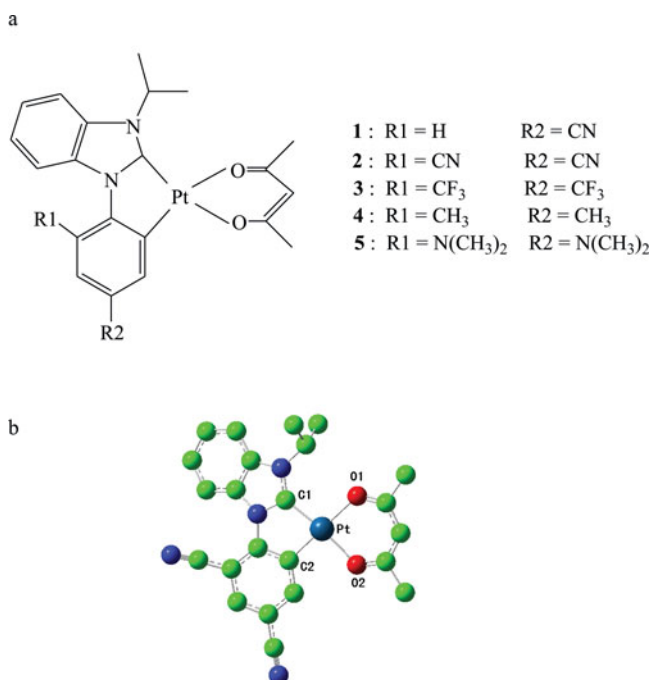5 : R1 = N(CH$_3$)$_2$ R2 = N(CH$_3$)$_2$

b

Figure 1. (a) Sketch map of the structures of platinum(II) complexes **1–5** (b) Representative optimized structure of **2** (H atoms omitted).

geometric structure for **2** is shown in Fig. 1b along with the numbering of some key atoms. The main geometric parameters in the ground and lowest triplet states are presented in Table S1 (Supplementary Information).

The calculated results show that the ground state geometries of complexes **1**−**5** display a slightly distorted planar construction. The carbon atom (C1 and C2) and the oxygen atom (O2 and O1) occupy the axial positions and coordinate with the center metal linearly as indicated from the calculated C1(C2)−Pt−O2(O1) angles greater than 170°. The optimized bond lengths and angles values are slightly larger than those from the experimental data. The discrepancy between our calculations and experiments is not only due to the fact that the crystal packing forces appeared in the experiment is not considered in the current calculations (performed on the single molecule), but it is well known that B3LYP overestimates the structural parameters (particularly bond lengths) in transition metal complexes.

The bond lengths of Pt−C1 in these complexes are shorter than those of Pt−C2. The reason may be that the imidazole group has a stronger electron donation ability to the metal d orbital than benzene group. It is also well-known that the nature of the behavior of the metal–ligand toward an empty d orbital of the metal and a concurrent back-donation will be from a filled d orbital to the π^* antibonding orbital of the ligand. In addition, it can be seen that the bond lengths of Pt-O1 are also longer than those of Pt-O2 for all these complexes. On the whole, from the singlet to the triplet excited state (T_1), geometries for these complexes retain with only slightly altered bond lengths around the platinum centre. It can be seen that the bond lengths of Pt−C2 for these complexes in T_1 state are relatively shorter compared with those in the S_1 state except for complex **4**.

3.2. Molecular orbital properties

It is well-known that the properties of the excited states and electronic transitions of organic light-emitting materials are closely related to the characters of the frontier molecular orbitals
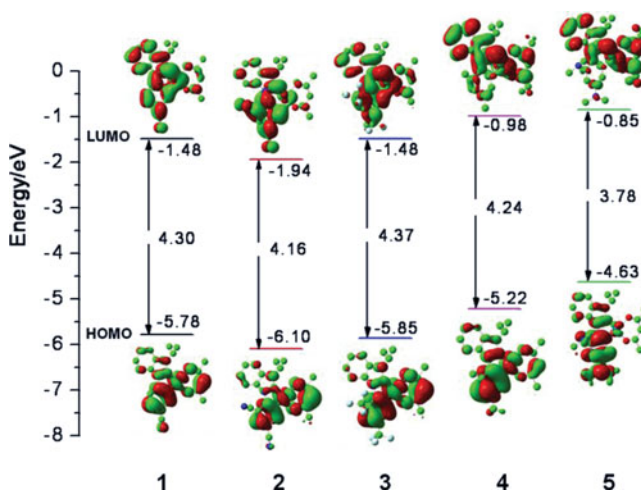
Figure 2. Molecular orbital diagrams and HOMO and LUMO energies for complexes **1–5**.

(FMOs), especially HOMO (highest occupied molecular orbital) and LUMO (lowest unoccupied molecular orbital). The HOMO and LUMO distribution, energy levels, and energy gaps between of LUMO and HOMO ($\Delta E_{L \to H}$) of the five complexes **1–5** are plotted in Fig. 2. The calculated FMOs compositions for **1–5** were listed in Tables S2–S6 (Supplementary Information).

The HOMO of complexes **1–4** reside on the whole complexes. For example, the HOMO of **1** is composed of Pt *d* orbital (27%), C^C ligand (53%), and O^O ligand (20%). But with respect to complex **5**, the HOMO distribution is mainly on the C^C ligand (97%). In addition, from Table S2–S6, it can also be seen that the LUMO of complexes **1–3** are mainly composed of Pt and C^C ligand. However, **4** and **5** have the LUMO distribution on the whole complexes. For example, the LUMO of **4** is composed of Pt d* orbital (13%), C^C ligand (69%), and O^O ligand (18%). Indeed, the orbital energy levels of HOMO and LUMO are affected by the different substituent groups on the phenyl ring moiety. It is obvious that the energies of HOMO and LUMO of complex **2** with the strong electron-accepting substituent group CN are the smallest among these complexes, i.e., –6.10 eV for HOMO and –1.94 eV for LUMO. The order of stabilization of the HOMO (LUMO) energy levels for complexes **2–5** is as follow: **2 < 3 < 4 < 5**, which means that the substituent groups with strong electron-donating ability on the phenyl ring moiety can raise the HOMO (LUMO) levels. From Fig. 2, it can be seen that **3** has the largest $\Delta E_{L \to H}$ value 4.37 eV among these complexes. In addition, the $\Delta E_{L \to H}$ of **5** with strong electron-donating substituent group N(CH$_3$)$_2$ is obvious smaller than those of complexes **1–4**.

3.3. *Ionization potential (IP) and electronic affinity (EA)*

In order to investigate the charge injection and transporting properties of luminescent materials, ionization potential (IP), electron affinity (EA), reorganization energy (λ), hole and electron extraction potential (HEP and EEP) have been calculated and presented in the Table 1. The details definitions for these physical quantities can be obtained from the previous work by others and us [29,30].

It is known that a larger EA (smaller IP) indicates easier injection of electrons (holes) into the emitting materials from the electron (hole) transporting layer. In Table 1, the IP value of

Table 1. The calculated vertical IP (IP$_v$), adiabatic IP (IP$_a$), HEP, vertical EA (EA$_v$), and adiabatic EA (EA$_a$), EEP, and reorganization energies for electron ($\lambda_{electron}$) and hole (λ_{hole}), unit: eV.

	IP$_v$	IP$_a$	HEP	EA$_v$	EA$_a$	EEP	$\lambda_{electron}$	λ_{hole}
1	7.130	7.016	6.890	0.218	0.329	0.458	0.240	0.239
2	7.424	7.329	7.224	0.653	0.792	0.960	0.306	0.200
3	7.208	7.077	6.924	0.210	0.416	0.768	0.558	0.283
4	6.613	6.443	6.257	-0.272	-0.090	0.382	0.655	0.356
5	5.999	5.579	5.344	-0.372	-0.185	0.267	0.639	0.654

complex **5** is the smallest one, which means that the hole injection is much easiest among these complexes. The EA value of complex **2** is the largest, which means the electron injection is much easier than the other complexes. The hole and electron injection and transport balance is important for the emitting layer material. The reorganization energy (λ) can be approximately used to estimate the charge transport rate and balance between holes and electrons. The complex **2** has the best hole transfer ability with the smallest λ_{hole} value (0.200 eV) among these complexes. As shown in Table 1, the $\lambda_{electron}$ values for all these complexes except **5** are larger than the λ_{hole} values, which suggests that the hole transfer rate is better than the electron transfer rate. It can also be seen that the difference between $\lambda_{electron}$ and λ_{hole} for complex **1** is the smallest among these complexes, which can greatly improve the charge transfer balance, thus further enhancing the device performance of OLEDs.

3.4. *Absorption spectra*

On the basis of the optimized ground state geometries, the absorption properties of complexes **1−5** were calculated using TDDFT method. The vertical electronic excitation energies, oscillator strengths (*f*), assignment, and configurations have been listed in Table S7 (Supplementary Information). The absorption spectra of the studied complexes in CH$_2$Cl$_2$ medium based on the TDDFT calculations are shown in Fig. 3.

The lowest energy absorption wavelengths are located at 346 nm (*f* = 0.0226) for **1**, 362 nm (*f* = 0.0586) for **2**, 344 nm (*f* = 0.0159) for **3**, 349 nm (*f* = 0.0018) for **4**, and 385 nm (*f* = 0.0566) for **5**, respectively. It can be seen that the lowest lying singlet → singlet absorption
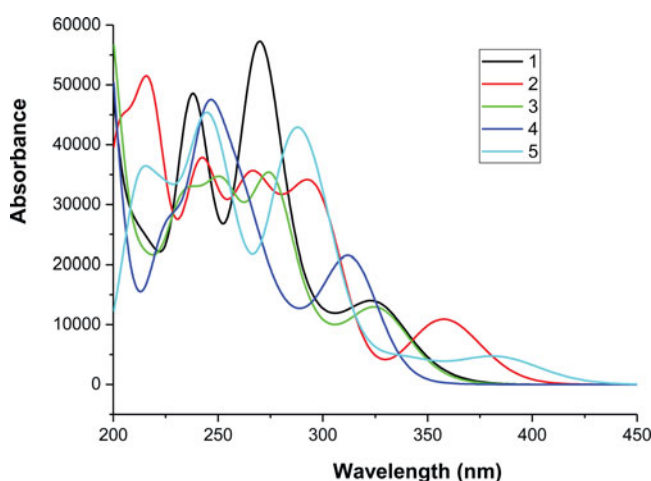
Figure 3. Simulated absorption spectra in CH$_2$Cl$_2$ medium for complexes **1–5**.

at 346 nm for **1** is comparable with the experimental value [18]. Indeed, the TDDFT calculations can predict the photophysical behavior of these Ir(III) complexes studied although it is generally believed to give substantial errors for the excitation energies of charge-transfer excited states [31]. The lowest lying absorption of complexes **2** and **5** are obviously red-shifted in contrast to those of other three complexes, which is consistent with the variation rules of the $\Delta E_{\text{L}\rightarrow\text{H}}$. Especially, the complex **5** has the maximum absorption wavelength 385 nm, which indicates that the strong electron-donating group $N(CH_3)_2$ has the obvious influence on the absorption properties. In addition, it can be seen from Table S7 that the lowest lying absorptions for all these complexes can be characterized as metal to ligand charge transfer (MLCT)/ ligand-to-ligand charge transfer (LLCT)/intraligand charge transfer (ILCT). From the Table S2–S7, it is interesting to note that the lowest lying absorptions of these complexes have the different transition characters. For example, the lowest lying absorptions of complexes **4** and **5** can be described as $d(Pt)+\pi(C^{\wedge}C)\rightarrow d^*(Pt)+\pi^*(C^{\wedge}C+O^{\wedge}O)$ and $\pi(C^{\wedge}C)\rightarrow d^*(Pt)+\pi^*(C^{\wedge}C+O^{\wedge}O)$ transitions. Meanwhile, Fig. 3 shows all these complexes have multiple absorption shapes at 200−350 nm wavelength.

3.5. *Phosphorescence*

The phosphorescent spectra in CH_2Cl_2 medium were calculated by TDDFT/M062X method on the basis of the optimized T_1 geometrical structures. The emission wavelengths, emission energies, and transition nature of complexes **1**–**5** calculated have been listed in Table 2. For comparison, the available experimental values are also listed.

From Table 2, it can be seen that complex **1** shows a theoretical band at 462 nm, **2** at 486 nm, **3** at 449 nm, **4** at 486 nm, and **5** at 531 nm. For **1**, the lowest energy emission (462 nm) is in good agreement with the experimental value (473 nm) [18]. The frontier molecular orbitals contours related to the emissions at 462, 486, 449, 486, and 531 nm, respectively, for complexes **1**–**5**, simulated in CH_2Cl_2 medium at M062X level have been presented in Fig. 4. In addition, partial frontier molecular orbital compositions (%) of complexes **1**–**5** in the triplet excited states have been present in Table S8. It is interesting that complexes **2** and **4** have the almost same emission wavelength 486 nm and different transition characters. The emission wavelength (531 nm) of complex **5** is obviously red-shifted in comparison to those of other four complexes, which is due to the strong electron-donating substituent group $N(CH_3)_2$ on the phenyl moiety in C^C ligand. From the Table 2, it can also be seen that the phosphorescences for complexes **1**, **2**, and **5** are mainly from the transitions of LUMO-HOMO configuration, which the calculated lowest emissions are described as ^{3}MLCT (metal to ligand charge transfer)/^{3}ILCT (intraligand charge transfer). For example, seen from Table S8, the emission transition character for **5** is assigned to ^{3}MLCT/^{3}ILCT $[d^*(Pt)+\pi^*(C^{\wedge}C)\rightarrow\pi(C^{\wedge}C)]$. As for

Table 2. Phosphorescent emissions of complexes **1**–**5** in CH_2Cl_2 medium at the TDDFT/M062X level, along with experimental wavelength (nm) available. (H Indicates HOMO, L Indicates LUMO).

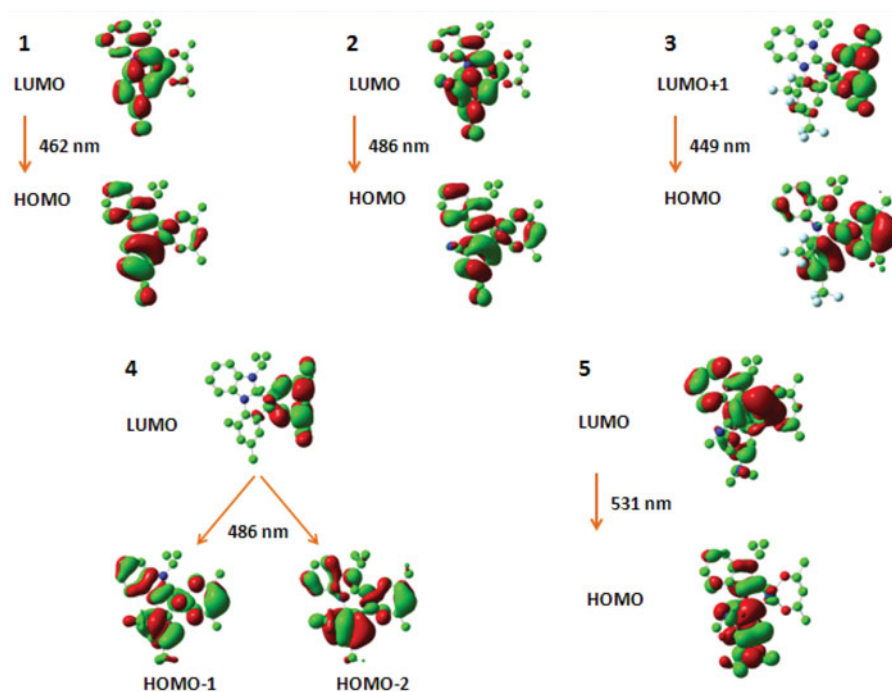|	λ (nm)/E (eV)	Configuration	Nature	Exptl.[a]
1	462/2.681	L→H(87%)	^{3}MLCT/^{3}ILCT	473
2	486/2.548	L→H(84%)	^{3}MLCT/^{3}ILCT	
3	449/2.758	L+1→H(70%)	^{3}MLCT/^{3}LLCT/^{3}ILCT	
4	486/2.550	L→H-1(51%)	^{3}MLCT/^{3}LLCT/^{3}ILCT	
		L→H-2(19%)	^{3}MLCT/^{3}LLCT/^{3}ILCT	
5	531/2.331	L→H(82%)	^{3}MLCT/^{3}ILCT	

[a] From Ref. [18].

Figure 4. Transitions responsible for the emissions at 462, 486, 449, 486, and 531 nm for complexes **1–5**, respectively, simulated in CH_2Cl_2 medium at the TDDFT/M062X levels.

3 and **4**, the dominant contribution for emissions are assigned to $^3MLCT/^3 \rightarrow LLCT$(ligand to ligand charge transfer)/^3ILCT transition characters.

3.6. *Phosphorescence quantum efficiency*

The emission quantum yield (Φ) can be affected by the competition between k_r (radiative decay rate) and k_{nr} (nonradiative decay rate), i.e., $\Phi = k_r/(k_r + k_{nr})$. It can be seen, to increase the quantum yield, k_r should be increased and k_{nr} should be decreased simultaneously or, respectively [32,33]. In addition, k_r is also theoretically related to the mixing between S_1 and T_1, which is proportional to the spin-orbit coupling (SOC) and inversely proportional to the energy gaps between the S_1 and T_1 states according to the following formula [34,35]:

$$k_r \approx \gamma \frac{\langle \psi_{S_1} | H_{S_0} | \psi_{T_1} \rangle^2 \mu_{S_1}^2}{(\Delta E_{S_1-T_1})^2} \tag{1}$$

$$\gamma = 16\pi^3 10^6 n^3 E_{em}^3/3h\varepsilon_0$$

where H_{S_0} is the Hamiltonian for the SOC, μ_{S_1} is the transition dipole moment in the $S_0 \rightarrow S_1$ transition, $\Delta E_{S_1-T_1}$ is the energy gaps between the S_1 and T_1 states, E_{em} represents the emission energy in cm^{-1} and n, h, and ε_0 are the refractive index, Planck's constant and the permittivity in a vacuum, respectively. Accordingly, the variation of quantum yield (Φ) can be qualitatively analyzed in theory from the above formula.

It is known that the phosphorescence quantum efficiencies could be increased by a larger ^3MLCT composition and thus the ISC. For platinum atom, the direct involvement of the d(Pt) orbital increases the first-order SOC in the $T_1 \rightarrow S_0$ transition and thus ISC, which would result

Table 3. The contribution of ^{3}MLCT (%) in the T$_1$ state and the energy gaps between the S_1 and T_1 states $\left(\Delta E_{S_1-T_1}\right)$ (in eV), along with the transition electric dipole moment in the $S_0 \rightarrow S_1$ transition μ_{S_1} (Debye), the radiative decay rate k_r ($\times 10^5$ s^{-1}) and nonradiative decay rate k_{nr} ($\times 10^5$ s^{-1}), together with the measured lifetime τ [μs] and quantum yields Φ [%] for the studied complex **1** in CH$_2$Cl$_2$ medium.

	^{3}MLCT	$\Delta E_{S_1-T_1}$	μ_{S_1}	Φ^a	τ^a	k_r^a	k_{nr}^a
1	4.35	0.80	0.25	63	9.7	0.644	0.378
2	9.24	0.81	0.69				
3	12.60	0.82	0.18				
4	8.72	0.69	0.02				
5	13.94	0.54	0.71				

[a]Ref. [18].

in a drastic decrease of the radiative lifetime and avoid the nonradiative process [36]. As presented by Chou et al. [37], the ^{3}MLCT can be calculated as follows:

$$CT(M) = \%(M)HOMO - x - \%(M)LUMO + y \qquad (2)$$

where $\%(M)HOMO - x$ and $\%(M)LUMO + y$ are electronic densities on the metal in HOMO$-x$ and LUMO$+y$. An increase of ^{3}MLCT character could enhance SOC and hence the transition probability which would result in a drastic decrease of the radiative lifetime and avoid the nonradiative process [38,39]. In Table 3, we have listed the ^{3}MLCT contributions which were calculated to be 4.35%, 9.24%, 12.60%, 8.72%, and 13.94% for complexes **1**–**5**, respectively. The ^{3}MLCT contributions of **1** and **5** are the smallest and largest among these complexes. It is also known that the phosphorescence quantum efficiencies are inversely proportional to the $\Delta E_{S_1-T_1}$ [40]. Namely, a minimal $\Delta E_{S_1-T_1}$ is required for enhancing the ISC rate, leading to the increased k_r. The $\Delta E_{S_1-T_1}$ for these complexes are also listed in Table 3, along with the μ_{S_1} values. The results give 0.80, 0.81, 0.82, 0.69, and 0.54 eV for $\Delta E_{S_1-T_1}$. The results give 0.25, 0.69, 0.18, 0.02, and 0.71 Debye for μ_{S_1}, respectively for **1**–**5**. From the aforementioned discussion, it is obvious that a lower $\Delta E_{S_1-T_1}$ and larger ^{3}MLCT contributions and higher μ_{S_1} values may account for a larger k_r according to Equation (1). From the data in Table 3, it can be seen that the complex **5** has possibly the larger k_r value than those of other complexes.

4. Conclusions

DFT and TDDFT calculations were conducted on a series of substituted platinum(II) complexes with a chelating NHC ligand (1-(4-cyanophenyl)-3-isopropyl-1H-benzo[d]imidazole and a bidentate monoanionic auxiliary ligand (acetylacetone) have to shed light on the influence of different substituted groups on their photophysical properties. The calculated absorption and phosphorescent properties of these complexes show a good agreement with the available experimental data. The calculated results shows that the electron-accepting and electron-donating substituted groups on the phenyl moiety in C^C ligangd have the important effect on the photophysical properties, such as absorption and emission spectra, charge-injection and -transport abilities, and phosphorescence efficiency. The calculated results show that the complex **5** possesses possibly the larger k_r value than those of other complexes. We hope that the theoretical investigation could be useful for designing the good phosphorescent platinum(II) material used in the OLEDs.

Acknowledgments

References

[1] Tsuboyama, A. *et al.* (2003). *J. Am. Chem. Soc.*, *125*, 12971.
[2] Liao, J. L. *et al.* (2014). *J. Mater. Chem. C*, *2*, 6269.
[3] Su, S. J., Cai, C., Takamatsu, J. & Kido, J. (2014). *Org. Electron.*, *13*, 1937.
[4] Che, C. M., Kwok, C. C., Lai, S. W., Rausch, A. F., Finkenzeller, W. J., Zhu, N. Y., & Yersin, H. (2010). *Chem. Eur. J.*, *16*, 233.
[5] Shang, X. H., Han, D. M., Zhan, Q., Zhou, D. F., & Zhang, G. (2015). *New J. Chem., 39*, 2588.
[6] Shang, X. H., Han, D. M., Wan, N., Zhou, D. F., & Zhang, G. (2015). *Chem. Phys. Lett., 635*, 217.
[7] Fukagawa, H., Shimizu, T., Hanashima, H., Osasa, Y., Suzuki, M., & Fujikake, H. (2012). *Adv. Mater.*, *24*, 5099.
[8] Fleetham, T., Wang, Z. X., & Li, J. (2012). *Org. Electron.*, *13*, 1430.
[9] Murphy, L., Brulatti, P., Fattori, V., Cocchi, M., & Williams, J. A. G. (2012). *Chem. Commun.*, *48*, 5817.
[10] Rossi, E., Murphy, L., Brothwood, P. L., Colombo, A., Dragonetti, C., Roberto, D., Ugo, R., Cocchi, M., & Williams, J. A. G. (2011). *J. Mater. Chem.*, *21*, 15501.
[11] Rausch, A. F., & Yersin, H. (2010). *Chem. Phys. Lett.*, *484*, 261.
[12] Wang, Z., Turner, E., Mahoney, V., Madakuni, S., Groy, T., & Li, J. (2010). *Inorg. Chem.*, *49*, 11276.
[13] Rausch, A. F., Thompson, M. E., & Yersin, H. (2009). *Chem. Phys. Lett.*, *468*, 46.
[14] Cocchi, M., Virgili, D., Fattori, V., Williams, J. A. G., & Kalinowski, J. (2007). *Appl. Phys. Lett.*, *90*, 023506.
[15] Williams, E. L., Haavisto, K., Li, J., & Jabbour, G. E. (2007). *Adv. Mater.*, *19*, 197.
[16] Brooks, J., Babayan, Y., Lamansky, S., Djurovich, P. I., Tsyba, I., Bau, R., & Thompson, M. E. (2002). *Inorg. Chem.*, *41*, 3055.
[17] Thomas III, S. W., Venkatesan, K., Müller, P., & Swager, T. M. (2006). *J. Am. Chem. Soc.*, *128*, 16641.
[18] Tronnier, A., Metz, S., Wagenblast, G., Muenster, I., & Strassner, T. (2014). *Dalton Trans.*, *43*, 3297.
[19] Tronnier, A., Pöthig, A., Metz, S., Wagenblast, G., Münster, I., & Strassner, T. (2014). *Inorg. Chem.*, *53*, 6346.
[20] Hohenberg, P., & Kohn, W. (1964). *Phys. Rev.*, *136*, B864.
[21] Becke, A. D. (1993). *J. Chem. Phys.*, *98*, 5648.
[22] Lee, C., Yang, W. T., & Parr, R. G. (1988). *Phys. Rev. B*, *37*, 785.
[23] Cancès, E., Mennucci, B., & Tomasi, J. (1997). *J. Chem. Phys.*, *107*, 3032.
[24] Cossi, M., Barone, V., Mennucci, B., & Tomasi, J. (1998). *Chem. Phys. Lett.*, *286*, 253.
[25] Hay, P. J., & Wadt, W. R. (1985). *J. Chem. Phys.*, *82*, 270.
[26] Hay, P. J., & Wadt, W. R. (1985). *J. Chem. Phys.*, *82*, 299.
[27] O'Boyle, N. M., Tenderholt, A. L., & Langner, K. M. (2008). *J. Comput. Chem.*, *29*, 839.
[28] Frisch, M. J. *et al.* (2009). *Gaussian 09*, Gaussian, Inc.: Wallingford, CT.
[29] Rienstra-Kiracofe, J. C., Tschumper, G. S., Schaefer, H. F., Nandi, S., & Ellison, G. B. (2002). *Chem. Rev.*, *102*, 231.
[30] Han, D. M., Zhang, G., Cai, H. X., Zhang, X. H., & Zhao, L. H. (2013). *J. Lumin.*, *138*, 223.
[31] Dreuw, A., & Head-Gordon, M. (2004). *J. Am. Chem. Soc.*, *126*, 4007.
[32] Fantacci, S., De Angelis, F., Sgamellotti, A., Marrone, A., & Re, N. (2005). *J. Am. Chem. Soc.*, *127*, 14144.
[33] Tamayo, A. B., Garon, S., Sajoto, T., Djurovich, P. I., Tsyba, L. M., Bau, R., & Thompson, M. E. (2005). *Inorg. Chem.*, *44*, 8723.

[34] Haneder, S., Da Como, E., Feldmann, J., Lupton, J. M., Lennartz, C., Erk, P., Fuchs, E., Molt, O., Munster, I., Schildknecht, C., & Wagenblast, G. (2008). *Adv. Mater.*, *20*, 3325.

[35] Turro, N. *Modern Molecular Photochemistry*, University Science Books: Palo Alto, USA, 1991.

[36] Yang, C. H., Cheng, Y. M., Chi, Y., Hsu, C. J., Fang, F. C., Wong, K. T., Chou, P. T., Chang, C. H., Tsai, M. H., & Wu, C. C. (2007). *Angew. Chem. Int. Ed.*, *46*, 2418.

[37] Cheng, Y. M., Li, E. Y., Lee, G. H., & Chou, P. T. (2007). *Inorg. Chem.*, *46*, 10276.

[38] Sprouse, S., King, K. A., Spellane, P. J., & Watts, R. J. (1984). *J. Am. Chem. Soc.*, *106*, 6647.

[39] Colombo, M. G., Brunold, T. C., Riedener, T., Güdel, H. U., Förtsch, M., & Büergi, H. B. (1994). *Inorg. Chem.*, *33*, 545.

[40] Avilov, I., Minoofar, P., Cornil, J., & De Cola, L. (2007). *J. Am. Chem. Soc.*, *129*, 8247.